Korean Journal of Radiology

Comparative Study between ZOOMit and Conventional Intravoxel Incoherent Motion MRI for Assessing Parotid Gland Abnormalities in Patients with Early- or Mid-Stage Sjögren's Syndrome

Qing-Qing Zhou[1]*, Wei Zhang[2]*, Yu-Sheng Yu[1], Hong-Yan Li[2], Liang Wei[1], Xue-Song Li[1], Zhen-Zhen He[1], Hong Zhang[1]

Departments of [1]Radiology and [2]Immunology and Rheumatology, The Affiliated Jiangning Hospital of Nanjing Medical University, Nanjing, China

Objective: To compare the reproducibility and performance of quantitative metrics between ZOOMit and conventional intravoxel incoherent motion (IVIM) magnetic resonance imaging (MRI) in the diagnosis of early- and mid-stage Sjögren's syndrome (SS).

Materials and Methods: Twenty-two patients (mean age ± standard deviation, 52.0 ± 10.8 years; male:female, 2:20) with early- or mid-stage SS and 20 healthy controls (46.9 ± 14.6 years; male:female, 7:13) were prospectively enrolled in our study. ZOOMit IVIM and conventional IVIM MRI were performed simultaneously in all individuals using a 3T scanner. Quantitative IVIM parameters - including tissue diffusivity (D), pseudodiffusion coefficient (D*), and perfusion fraction (f) - inter- and intra-observer reproducibility in measuring these parameters, and their ability to distinguish patients with SS from healthy individuals were assessed and compared between ZOOMit IVIM and conventional IVIM methods, appropriately. MR gland nodular grade (MRG) was also examined.

Results: Inter- and intra-observer reproducibility was better with ZOOMit imaging than with conventional IVIM imaging (ZOOMit vs. conventional, intraclass correlation coefficient of 0.897–0.941 vs. 0.667–0.782 for inter-observer reproducibility and 0.891–0.968 vs. 0.814–0.853 for intra-observer reproducibility). Significant differences in ZOOMit f, ZOOMit D*, conventional D*, and MRG between patients with SS and healthy individuals (all $p < 0.05$) were observed. ZOOMit D* outperformed conventional D* in diagnosing early- and mid-stage SS (area under receiver operating curve, 0.867 and 0.658, respectively; $p = 0.002$). The combination of ZOOMit D*, MRG, and ZOOMit f as a new diagnostic index for SS, increased diagnostic area under the curve to 0.961, which was higher than that of any single parameter (all $p < 0.01$).

Conclusion: Considering its better reproducibility and performance, ZOOMit IVIM may be preferred over conventional IVIM MRI, and may subsequently improve the ability to diagnose early- and mid-stage SS.

Keywords: *Sjögren's syndrome; Parotid gland; Magnetic resonance imaging; Intravoxel incoherent motion; ZOOMit*

INTRODUCTION

Sjögren's syndrome (SS) is a chronic systemic autoimmune disease [1] associated with significant xerostomia and xerophthalmia, while the parotid glands are the most frequently involved exocrine glands [2]. Currently, the 2016 American College of Rheumatology (ACR) and the European League Against Rheumatism (EULAR) classification criteria are the main diagnostic criteria for SS [3]. These criteria are based on clinical xerostomia and xerophthalmia, serology,

labial salivary gland (LSG) biopsy, and ocular staining score (OSS) of keratoconjunctivitis sicca [4]. However, clinical symptoms are subject to strong subjectivity (patients with SS diagnosis may be characterized by mild parotid symptoms without parotid gland swelling [5]). Furthermore, the diagnostic criteria are complex; for example, OSS assessment is complicated and LSG biopsy is invasive and has a low acceptance rate. Hence, cases with missed diagnoses are common [6], which is detrimental to the early diagnosis and treatment of patients.

Because of its noninvasive, radiation-free nature and sensitivity to morphological and functional changes of the parotid glands, MRI has become a potential assessment tool for SS [1,7,8]. For late-stage SS (gland fat deposition [Gf] grade 3 or 4 [9], parotid gland atrophy with substantial adipose deposition), morphological changes are relatively easy to detect with conventional MRI and MR sialography (MRS); however, these methods are not very sensitive for detection of early-stage SS (Gf grade 0 or 1, normal parotid gland appearance with no or only slight fat deposition) [2,8].

Recently, intravoxel incoherent motion (IVIM) MRI is demonstrably more effective for diagnosing early-stage SS [2,8], parotid gland tumors [10], or evaluation of irradiated salivary gland dysfunction [11-14]. However, large-field imaging was applied in all previous studies, which is relatively restricted in displaying small structures of organs or small changes due to disease [15,16]. ZOOMit technology simultaneously employs two parallel radiofrequency pulse sequences. It minimizes the negative effects of folding artifacts and provides high image quality, decreased distortion and blurring, decreased motion and flow artifacts, and increased spatial resolution [17-19]. Nonetheless, to our knowledge, no studies have evaluated the parotid glands with ZOOMit IVIM in patients with SS.

Consequently, our study aimed to investigate whether IVIM parameters, including the diffusion coefficient (D), pseudodiffusion coefficient (D*) and perfusion fraction (f), assessed with ZOOMit imaging could better identify subtle abnormalities in the parotid gland, compared to that identified via conventional imaging. We also assessed the inter- and intra-observer reproducibility in measuring ZOOMit and conventional IVIM parameters. We compared the diagnostic performance of these two technical IVIM methods for diagnosing early- or mid-stage SS and selected the most valuable diagnostic indicators.

MATERIALS AND METHODS

The study was performed after approval from the Institutional Review Board (IRB No. 2020-03-018-K01) of The Affiliated Jiangning Hospital of Nanjing Medical University, and informed consent was obtained from every participant.

Study Population

We prospectively recruited 27 consecutive SS patients from January to July 2020. SS was diagnosed based on the 2016 ACR/EULAR classification criteria [3]. The exclusion criteria were: 1) late-stage SS (Gf grade 3 or 4) [9], 2) recent acute infection of the salivary glands (within 1 week), 3) diabetes, smoking, 4) benign/malignant tumors, and 5) MRI scans with various artifacts leading to poor image quality. Finally, 18 early-stage SS (Gf grade 0 or 1) and 4 middle-stage SS (Gf grade 2) patients were enrolled in the study. Four patients with late-stage SS and one patient with poor image quality were excluded. Moreover, 20

Table 1. MRI Protocols for ZOOMit and Conventional Imaging

| MRI Protocols	ZOOMit	Conventional
Repetition time, msec (shortest)	5200	4200
Echo time, msec (shortest)	92	60
Matrix	190 x 190	142 x 114
Slices	18	18
Slice thickness, mm	4	4
Slice gap, mm	0.8	0.8
Field of view, cm	24 x 24	18 x 9
Voxel size, mm	0.6 x 0.6	0.6 x 0.6
Acquisition time	6 minutes 42 seconds	6 minutes 31 seconds
B values, s/mm^2	0, 30, 60, 90, 120, 150, 200, 400, 800	
Number of excitations	Two signal averages were chosen for a b value less than 200 s/mm^2, four for a b value less than 400 s/mm^2 and eight for a b value less than 800 s/mm^2	

healthy control (HC) individuals were included in this study.

Clinical Information Collection

Oral tests, ocular tests, and serological assays were performed for SS diagnosis. Oral tests included LSG biopsy to determine the focus score (FS) of focal lymphocytic sialadenitis. Ocular tests comprised of the binocular Schirmer test and OSS. Serological assays included evaluations of anti-Sjögren's syndrome A/B (SSA/SSB), antinuclear antibody (ANA) titers, rheumatoid factor, immunoglobulin G, and the presence of complement C3 and C4 [3]. Clinical data collection and SS diagnosis were performed by one rheumatologist (with 12 years of clinical experience).

MRI Examinations

All MRI examinations were performed with a 3T MRI scanner (Prisma, Siemens). All participants were asked to fast for at least 2 hours before the MRI examination. Participants were placed in the supine position, and the head and neck were fixed with dedicated pads in a 64-channel head coil. Participants were asked to minimize swallowing during the scan. In addition to conventional axial T1 weighted image (T1WI), DIXON-T2-weighted imaging (DIXON-T2WI, spin echo sequence based dual-echo water-fat separation technology), and MRS, all individuals underwent conventional and ZOOMit (Siemens Medical) IVIM simultaneously for a pretreatment assessment. Table 1 summarizes the detailed MRI protocols
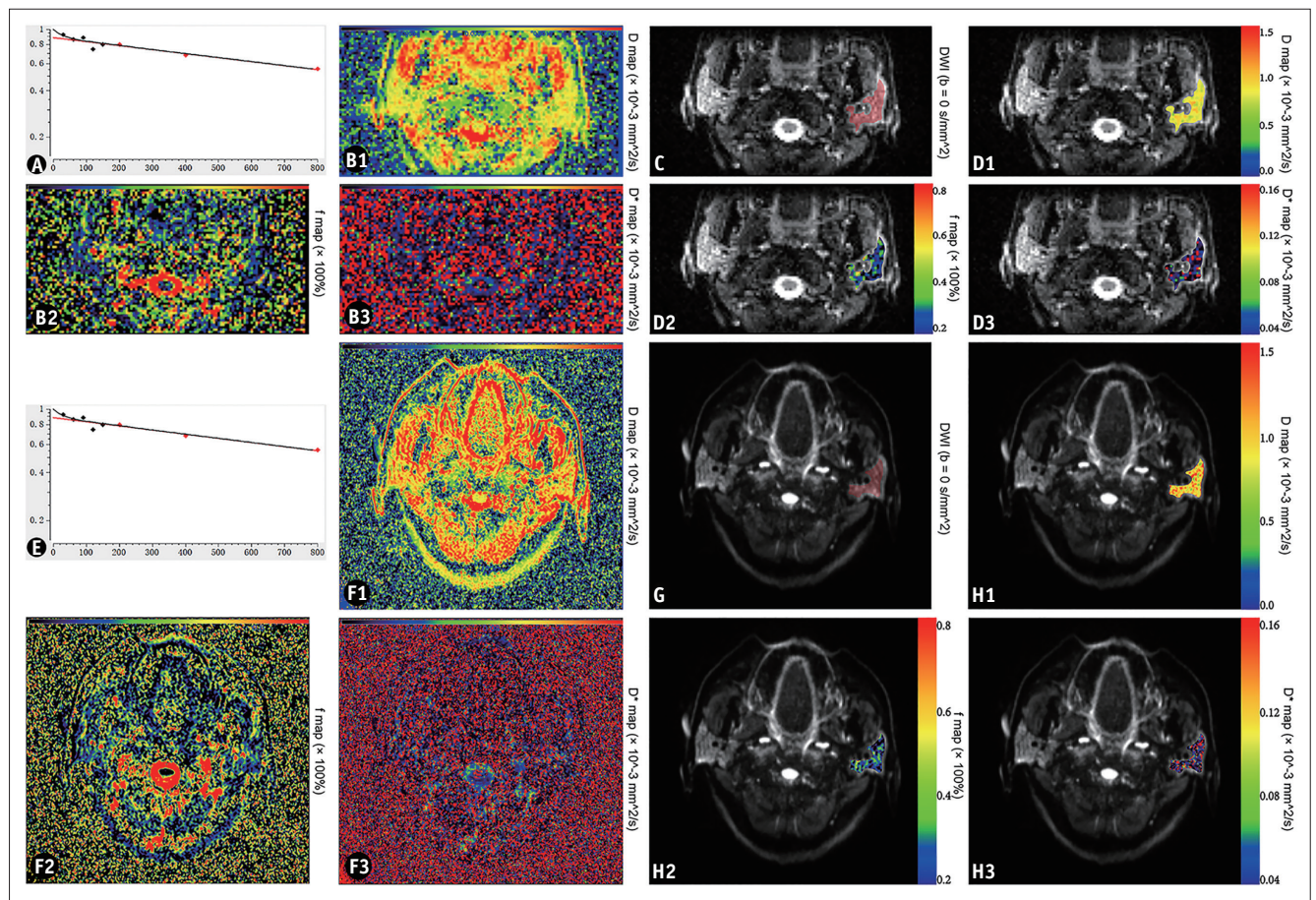
Fig. 1. Analysis process for ZOOMit and conventional IVIM imaging.
A. Maximum overlap of the IVIM curve and the fitting line of ZOOMit IVIM images. **B1-3.** The generated D, f, and D* maps of ZOOMit IVIM images. **C.** The ROI was placed at least 2 mm from the left parotid margin on the ZOOMit DWI scan (b = 0 s/mm²). **D1-3.** The same ROI was placed on the D, f, and D* maps of ZOOMit IVIM images to obtain the corresponding Z-D, Z-f, and Z-D* values, respectively. **E.** Maximum overlap of the IVIM curve and the fitting line of conventional IVIM images. **F1-3.** The generated D, f, and D* maps of conventional IVIM images. **G.** The ROI was placed at least 2 mm from the left parotid margin on a conventional DWI image (b = 0 s/mm²). **H1-3.** The same ROI was placed on the D, f, and D* maps of conventional IVIM images to obtain the corresponding C-D, C-f, and C-D* values, respectively. C-D = conventional diffusion coefficient, C-D* = conventional pseudodiffusion coefficient, C-f = conventional perfusion fraction, DWI = diffusion-weighted imaging, IVIM = intravoxel incoherent motion, ROI = region of interest, Z-D = ZOOMit diffusion coefficient, Z-D* = ZOOMit pseudodiffusion coefficient, Z-f = ZOOMit perfusion fraction

for ZOOMit and conventional imaging. All scan sequences were performed from the sella turcica to the submandibular glands, covering the entire volume of the bilateral parotid glands.

Image Analysis

Two radiologists with seven and four years of experience in head and neck MRI diagnosis analyzed the MR images on the picture archiving and communication system. They were blinded to the clinical information and study design. The MR gland nodular grade (MRG) of the parotid glands was evaluated independently based on the MRS findings, according to the scale reported by Makula et al. [20]. If the conclusion was inconsistent, a third senior radiologist with 16 years of experience in head and neck radiology contributed to the discussion, until a consensus was attained.

The IVIM dataset was calculated based on the biexponential model introduced by Le Bihan et al. [21] with the following formula: $Sb/S0 = (1 - f) \times exp (-b \times D) + f \times exp (-b \times (D^* + D))$, in which S0 represents the mean signal intensity when $b = 0$ s/mm^2, and Sb represents the mean signal intensity with diffusion gradient b. IVIM data were postprocessed using the MITK Diffusion software (version: 2014.10.2, available at http://mitk.org/wiki/MITK). IVIM fitting was performed in a stepwise manner, and a cutoff b-value of 170 s/mm^2 was applied. The most suitable images were adjusted to maximize the overlap between the IVIM curve and the fitting line (Fig. 1A, E). Subsequently, the D, f, and D* maps were generated automatically and saved in Nifti format (Fig. 1B, F). Three polygonal regions of interest (ROIs) were drawn freehand on the largest slice of the parotid gland, and the neighboring upper and lower slices of the DWI scans ($b = 0$ s/mm^2) using MRIcron software (available at http://www.mricro.com). ROIs were placed at least 2 mm from the parotid margin to avoid field inhomogeneity and susceptibility artifacts. The retromandibular vein, maxillary artery and maxillary veins were also avoided (Fig. 1C, G). Then, the three ROIs were saved and copied to D, f, and D* maps to obtain the corresponding D, f, and D* values (Fig. 1D, H). The bilateral parotid glands of all individuals were measured separately. The mean values of the three ROIs comprised the IVIM parameter values for each unilateral parotid gland, and the averages of the values assigned by the two observers were calculated as the final values. Repeated measurements were performed by one radiologist after two months, for reproducibility analyses.

Statistical Analysis

The intra- and inter-observer reproducibility was assessed using intraclass correlation coefficient (ICC) values. The independent sample t test or Wilcox test was used to compare IVIM parameters between the right and left parotid glands and to compare ZOOMit and conventional imaging IVIM parameters between the two groups, respectively. Pearson linear correlation was used to evaluate the correlation between significant IVIM parameters and the serological assay results. Receiver operating characteristic (ROC) curve, area under the curve (AUC), and sensitivity and specificity analyses were employed to assess the diagnostic efficiency of ZOOMit and conventional IVIM parameters. AUC values were compared using Delong test. A two-tailed $p < 0.05$ was considered statistically significant. Statistical analyses and graphing were performed in R 4.0.2 (the R Foundation for Statistical Computing).

RESULTS

Study Population Characteristics

Twenty-two SS patients and 20 HCs were involved in our study. There were no significant differences in terms of sex ($p = 0.062$) or age ($p = 0.231$) between the two groups. The patients' general characteristics, clinical information, and radiographic staging are summarized in Table 2.

Table 2. The Patient's General, Clinical Information and Radiographic Staging

	SS Group (n = 22)	HC Group (n = 20)	P
Age, mean ± SD	52.0 ± 10.8	46.9 ± 14.6	0.231
Sex, male:female	2:20	7:13	0.062
MRG (0, 1, 2, 3)*	11, 8, 3, 0	20, 0, 0, 0	< 0.001
Early-stage (Gf grade 0 or 1)	18		
Middle-stage (Gf grade 2)	4		
Clinical information			
Ocular staining score	6.68 ± 2.64		
Schirmer	3.54 ± 0.95		
Anti-SSA+	13		
ANA+	15		
Focus score (1, 2, 3, 4)	2, 3, 4, 13		

Data are mean ± SD or number of subjects. *MRG was significantly higher in the SS group than in the HC group (Fisher test: $p < 0.001$). ANA+ = antinuclear antibody positivity, Anti-SSA+ = anti-Sjögren's syndrome A positivity, Gf = Gland fat deposition, HC = healthy control, MRG = MR gland nodular grade, SD = standard deviation, SS = Sjögren's syndrome
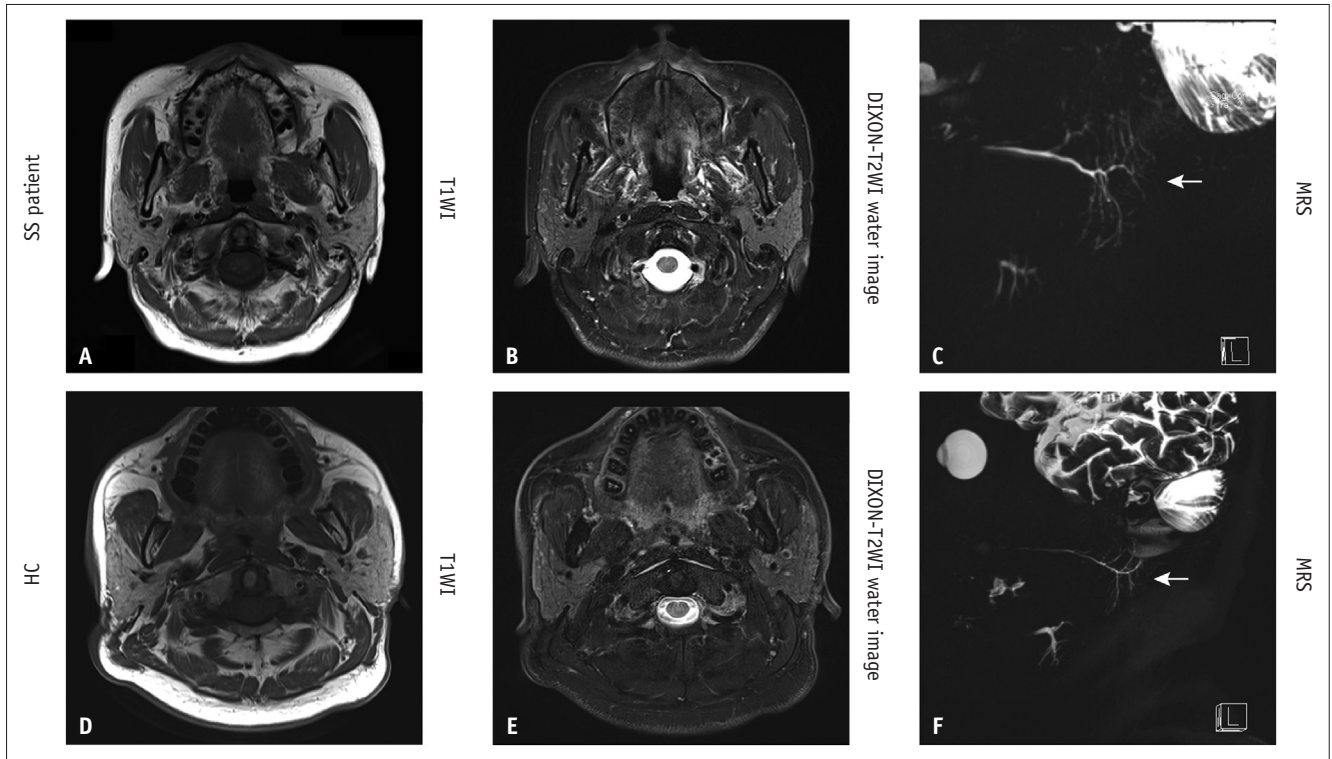
Fig. 2. Representative cases of SS patients and HCs without morphological or MRI signal changes of the parotid gland.
A-C. Axial T1WI, T2-weighted DIXON water image and MRS of a 52-year-old female patient with SS (Gf grade 0, MRG 1). The white arrow indicates fine reticular or small nodular structure of MRS in **(C)**. **D-F.** Axial T1WI, T2-weighted DIXON water image and MRS of a 57-year-old male HC (Gf grade 0, MRG 0). The white arrow indicates normal MRS in **(F)**. DIXON-T2WI = DIXON T2-weighted imaging, Gf = Gland fat deposition, HC = healthy control, MRG = MR gland nodular grade, MRS = MR sialography, SS = Sjögren's syndrome, T1WI = T1-weighted imaging

Representative cases of early-stage SS patients (Gf grade 0, MRG 1) and HCs (Gf grade 0, MRG 0) without morphological and MRI signal changes of the parotid gland are shown in Figure 2.

Observer Reproducibility

Intra- and inter-observer reproducibility was better with ZOOMit imaging than were those observed with conventional imaging, based on ICC values (Table 3).

Comparison of Parameters between the SS and HC Groups

Among the ZOOMit IVIM parameters (Z-D, Z-f, Z-D*) and conventional IVIM parameters (C-D, C-f, C-D*), the C-D value exhibited a slight but significant difference between the right and left parotid glands in patients with SS (p = 0.021), while no significant differences were found in other parameters (Table 4).

For the 84 parotid glands in 42 individuals, significant differences in the Z-f, Z-D*, and C-D* values between the SS and HC groups were observed (Z-f: 0.15 > 0.11, p < 0.001; Z-D*: 54.25 x 10^{-3} mm^2/s > 40.67 x 10^{-3} mm^2/s, p < 0.001;

Table 3. Intra- and Interobserver ICCs for the Measurements Derived from Conventional and ZOOMit IVIM Images of Parotid Glands

Parameter	Interobserver ICC	Intraobserver ICC
ZOOMit IVIM parameters		
D, 10^{-3} mm^2/s	0.941 (0.893, 0.988)	0.968 (0.929, 0.992)
f, %	0.921 (0.882, 0.954)	0.934 (0.889, 0.983)
D*, 10^{-3} mm^2/s	0.897 (0.841, 0.936)	0.891 (0.838, 0.923)
Conventional IVIM parameters		
D, 10^{-3} mm^2/s	0.748 (0.541, 0.935)	0.853 (0.742, 0.958)
f, %	0.667 (0.543, 0.788)	0.814 (0.696, 0.933)
D*, 10^{-3} mm^2/s	0.782 (0.684, 0.875)	0.827 (0.747, 0.916)

Data in parentheses are the 95% confidence intervals. D = diffusion coefficient, D* = pseudodiffusion coefficient, f = perfusion fraction, ICC = intraclass correlation coefficient, IVIM = intravoxel incoherent motion

C-D*: 51.32 x 10^{-3} mm^2/s > 47.19 x 10^{-3} mm^2/s, p = 0.013). Additionally, MRG was significantly higher in the SS than in the HC group (p < 0.001). IVIM parameters and MRG results were compared between the two groups and are summarized in Table 5. Figure 3 presents the differences in the Z-f, Z-D*, and C-D* values from the cases included in

Table 4. Comparison of ZOOMit and Conventional Intravoxel Incoherent Motion Parameters between the Left and Right Parotid Glands

	ZOOMit			Conventional		
	D	f	D*	D[a]	f	D*
SS group						
R	0.69 ± 0.12	0.14 ± 0.04	55.21 ± 9.65	0.90 ± 0.16	0.17 ± 0.05	49.46 ± 7.41
L	0.69 ± 0.12	0.16 ± 0.04	53.28 ± 9.72	0.79 ± 0.14	0.18 ± 0.05	53.17 ± 5.70
p value	0.840	0.126	0.511	0.021	0.434	0.070
HC group						
R	0.70 ± 0.11	0.10 ± 0.03	39.19 ± 6.34	0.86 ± 0.12	0.19 ± 0.06	48.58 ± 5.47
L	0.74 ± 0.09	0.11 ± 0.03	42.14 ± 5.05	0.80 ± 0.21	0.18 ± 0.05	45.79 ± 10.62
p value	0.142	0.167	0.112	0.280	0.408	0.204

Data are mean ± standard deviation. [a]The D value exhibited a slight difference between the right and left SS parotid glands ($p = 0.021$). D = diffusion coefficient, D* = pseudodiffusion coefficient, f = perfusion fraction, HC = healthy control, SS = Sjögren's syndrome

Table 5. Comparison of ZOOMit and Conventional IVIM Parameters between SS and HC Groups

	SS Group (n = 22)	HC Group (n = 20)	P
ZOOMit IVIM parameters			
D, 10^{-3} mm^2/s	0.69 ± 0.12	0.72 ± 0.10	0.400
f, %*	0.15 ± 0.04	0.11 ± 0.29	< 0.001
D*, 10^{-3} mm^2/s*	54.25 ± 9.62	40.67 ± 5.85	< 0.001
Conventional IVIM parameters			
D, 10^{-3} mm^2/s	0.85 ± 0.15	0.83 ± 0.17	0.641
f, %	0.18 ± 0.05	0.18 ± 0.57	0.585
D*, 10^{-3} mm^2/s[†]	51.32 ± 6.80	47.19 ± 8.46	0.013

Data are mean ± standard deviation or number of subjects. *The ZOOMit f and D* values of the SS group were significantly higher than those of the HC group (Wilcox test: all $p < 0.001$), [†]The conventional D* value of the SS group was significantly higher than that of the HC group (Wilcox test: $p = 0.013$). D = diffusion coefficient, D* = pseudodiffusion coefficient, f = perfusion fraction, HC = healthy control, IVIM = intravoxel incoherent motion, SS = Sjögren's syndrome

Figure 2.

Correlation Analysis

Pearson correlation was used to evaluate the correlation between the IVIM parameters with significant differences between groups and serological assay results. However, no significant correlations were found between IVIM parameters and serological assay results (all correlation coefficients < 0.3, and all p values > 0.01) (Supplementary Table 1).

## Comparison of Diagnostic Efficiency between ZOOMit and Conventional Imaging

MRG and IVIM parameters derived from ZOOMit and conventional imaging with differences between subgroups (including Z-f, Z-D*, and C-D*) were selected as diagnostic indexes. ROC analysis indicated that Z-D* had the best diagnostic performance for detecting early- and mid-stage SS (AUC = 0.867, 95% confidence interval [CI]: 0.786–0.948), followed by Z-f (AUC = 0.780, 95% CI: 0.682–0.879), MRG (AUC = 0.750, 95% CI: 0.675–0.825) and C-D* (AUC = 0.658, 95% CI: 0.540–0.776). Although a significant difference was found in diagnostic performance between Z-D* and C-D* (AUC, 0.867 vs. 0.658, DeLong test: $p = 0.002$), there was no statistically significant difference between any other metric pairs (DeLong test: all $p > 0.05$).

When Z-D*, Z-f, and MRG were combined as a new diagnostic index for SS, the AUC reached 0.961 (95% CI: 0.912–1.000), and sensitivity and specificity for diagnosing SS (with the cutoff values of Z-D* > 51.25 mm^2/s, Z-f > 0.12, and MRG > 1 according to maximum Youden index) were 90.9% and 100.0%, respectively. The Delong test demonstrated that the diagnostic efficiency of the combined index was greater than that of any single diagnostic metric (all $p < 0.01$) (Fig. 4).

DISCUSSION

Our study demonstrated that the IVIM parameters of ZOOMit imaging could better monitor the subtle difference between early- and mid-stage SS patients and HCs, compared to conventional imaging. ZOOMit IVIM parameters (Z-D* and Z-f) had higher reproducibility and diagnostic efficiency than conventional IVIM parameters (C-D*). Furthermore, the AUC of the combination of Z-D*, Z-f, and MRG for diagnosing SS reached 96.1%, which was significantly higher than that of conventional IVIM
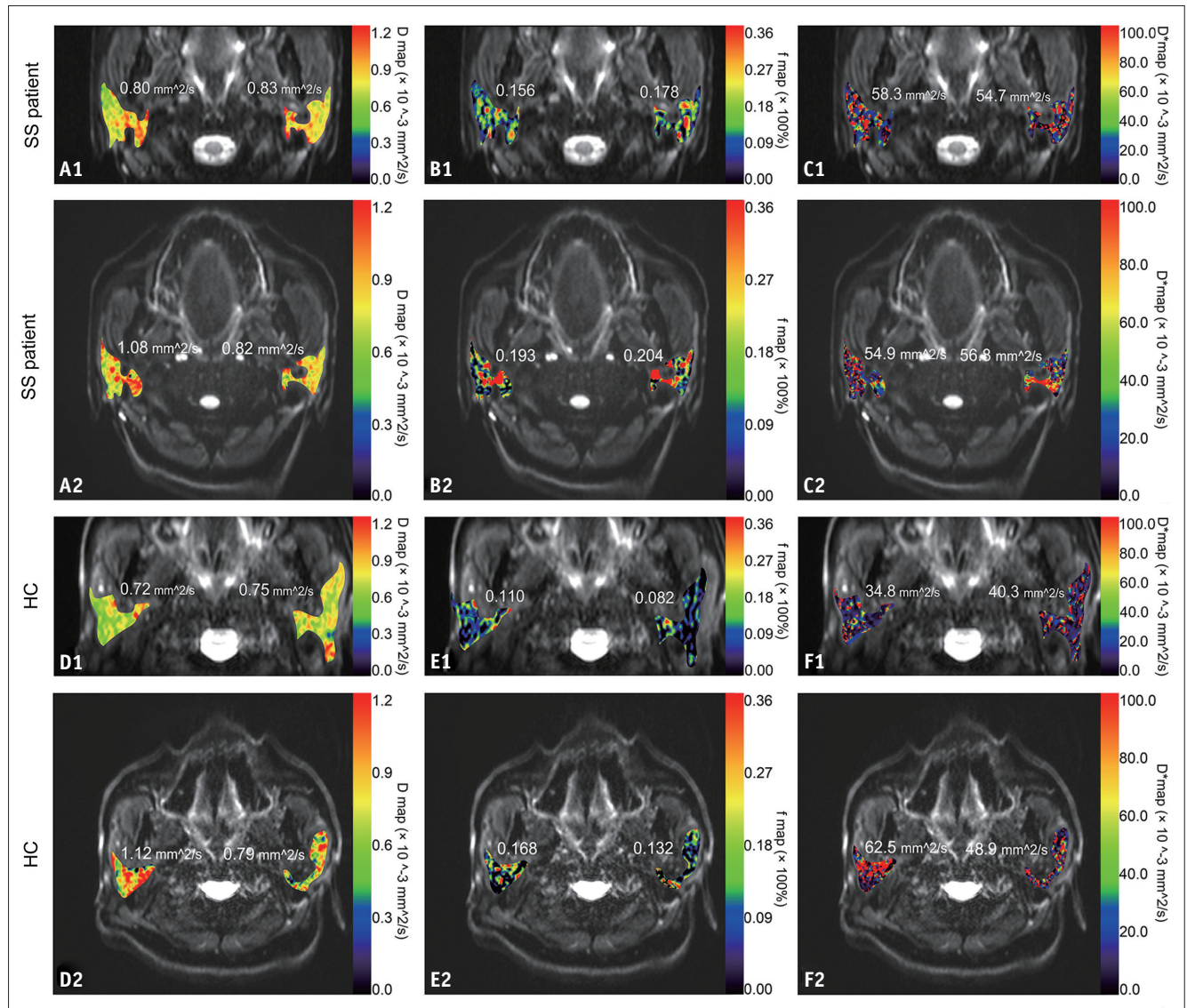
Fig. 3. Differences in the Z-f, Z-D*, and C-D* values of the two identical cases shown in Figure 2. Z-D, Z-f, and Z-D* maps **(A1-C1)** and C-D, C-f, and C-D* maps **(A2-C2)** of a 52-year-old female SS patient. Z-D, Z-f, and Z-D* maps **(D1-F1)** and C-D, C-f, and C-D* maps **(D2-F2)** of a 57-year-old male HC. The Z-f value of the SS patient was higher than that of the HC, and SS can be correctly diagnosed with a Z-f value greater than 0.120 in both the left and right parotid glands **(B1)**. The Z-D* value of the SS patient was higher than that of the HC, and SS can be correctly diagnosed with a Z-D* value greater than 51.25 mm²/s in both the left and right parotid glands **(C1)**. The C-D* value was high in both the SS patient and HC, and the right normal parotid gland was misdiagnosed as SS. C-D = conventional diffusion coefficient, C-D* = conventional pseudodiffusion coefficient, C-f = conventional perfusion fraction, D = diffusion coefficient, D* = pseudodiffusion coefficient, f = perfusion fraction, HC = healthy control, SS = Sjögren's syndrome, Z-D = ZOOMit diffusion coefficient, Z-D* = ZOOMit pseudodiffusion coefficient, Z-f = ZOOMit perfusion fraction

parameters and values reported in previous studies.

In terms of conventional IVIM parameters, only the D* value exhibited differences between subgroups. However, for ZOOMit IVIM parameters, Z-f, and Z-D* values were strikingly different between subgroups, probably due to the essential technical differences between ZOOMit and conventional IVIM MRI. In ZOOMit imaging, parallel imaging techniques have become widely used to reduce distortions

and the physical field of view (FOV) [22]. Zoomed EPI techniques further reduce artifacts by applying two dimensional spatially selective excitation pulses to limit the size of the FOV in the phase-encoding direction. In addition to B1 shimming, the 2-channel parallel RF transmission system allows for a significant reduction in FOV in the phase encoding direction [23,24]. This reduction in FOV and the number of phase-encoding steps can, in turn,
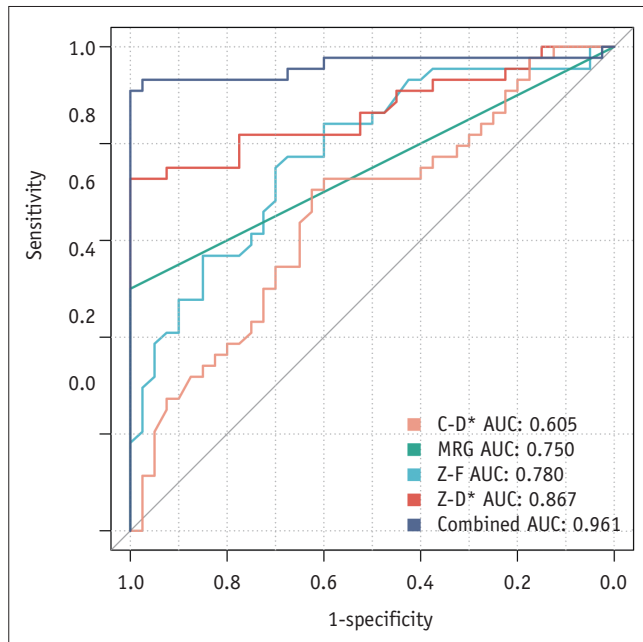
Fig. 4. Receiver operator characteristic curves of MRG and Z-D*, Z-f, and C-D* values for diagnosis of early- and mid-stage SS. The Delong test demonstrated that the diagnostic efficiency of the combined indicators was greater than that of any single diagnostic indicator (all $p < 0.01$). AUC = area under the curve, C-D* = conventional pseudodiffusion coefficient, MRG = MR gland nodular grade, Z-D* = ZOOMit pseudodiffusion coefficient, Z-f = ZOOMit perfusion fraction

reduce image distortion and other phase-encoding-related artifacts, as well as increase the spatial resolution, thereby further improving the image quality. Moreover, by drawing ROIs on the higher-resolution ZOOMit images and comparing them with the corresponding regions on conventional lower-resolution IVIM images, radiologists can more accurately distinguish the boundaries of the parotid gland and efficiently avoid the retromandibular vein, maxillary artery and maxillary veins of the parotid gland. Therefore, ZOOMit IVIM imaging can monitor the subtle differences in IVIM values between subgroups. Furthermore, due to its low resolution, conventional IVIM imaging showed lower intra- and inter-observer reproducibility than ZOOMit imaging, which may further lead to inconsistent Z-D values in the left and right parotid glands.

Both the f and D* values were significantly higher in the early- and mid-stage SS group than in the HC group, consistent with previous studies [2,8]. Su et al. [8] demonstrated that the f and D* values of parotid glands were significantly higher in patients with early-stage SS than in healthy individuals. Chu et al. [2] showed that both the f and D* values of parotid glands were significantly higher in SS patients than in healthy volunteers, except

for patients with MRG 3. The f value is a measure of the fractional volume of capillary blood flowing in each voxel and is thought to be an indicator of vascular permeability [25], while D* is determined via the signal intensity ratios of the blood capillaries and considered to be related to tissue vascularity [12]. The results from these studies were obviously consistent with the histopathological changes of SS, such as inflammation, gland edema, and increased vascular permeability [2,8,26]. However, in these studies [2,8], the D value was higher in SS patients than in HCs, while in our study, it was lower in SS patients. The reason may be that the degree of lymphocyte infiltration, glandular tissue damage, excretory duct vacuolation, and fibrous tissue proliferation varies between different stages of SS, possibly leading to great variations in the D value—which reflects the free diffusion of water molecules—between different SS stages.

When the relationship between IVIM parameters and clinical serum values was further analyzed, no correlations were found. In our clinical practice, we could observe that the parotid glands were only mildly involved in almost half of the SS patients, despite the fact that they had suffered from severe extraglandular symptoms, such as peripheral neuropathy, arthritis, and hematological manifestations. Extraglandular involvement would result in elevated serum values; however, the MRI parameters of the parotid glands would not increase accordingly due to the mild involvement. Therefore, quantitative MRI metrics of the parotid glands were not significantly correlated with clinical serum values in SS patients. Furthermore, we reviewed the clinical information of all 22 SS patients and found that two SS patients were negative for anti-SSA/Ro, and one SS patient had negative LSG biopsies based on the FS, although these patients were diagnosed correctly using a combination of quantitative MRI metrics. Among the 22 SS patients who underwent clinical testing, the rate of missed diagnosis for serology was 9.1% (2/22). The rate of missed diagnosis for LSG biopsy was 4.5% (1/22), which is close to the 2.5% reported in the published literature [27]. This further confirms the important clinical value of quantitative MRI metrics as an effective supplement for SS diagnosis, especially that of ZOOMit IVIM parameters, which show excellent reproducibility and thus have a higher diagnostic performance than conventional IVIM parameters.

Our study had the following four advantages: 1) all previous studies on SS and IVIM adopted the American-European Consensus Group classification criteria from 2002,

while our study adopted the ACR and EULAR classification criteria from 2016, 2) in our study, both ZOOMit and conventional images were acquired for all patients, thus avoiding individual differences, 3) the diagnostic performance of the combination of Z-D*, Z-f, and MRG as indicators for SS was significantly higher than the diagnostic efficacy of other indicators in previous similar studies [8], and 4) all SS patients were characterized by early- and mid-stage disease, thus circumventing the possible effects of adipose tissue on IVIM parameters observed in patients with late-stage SS [28]. However, our study also had some limitations. First, the sample size was relatively small, and the distribution of each MRG among patients was uneven. Therefore, we could not classify patients according to MRG. Additional studies with increased number of MRG 1–3 patients would stratify patients by MRG to explore changes in ZOOMit IVIM parameters. Second, although SS is a diffuse disease, which was also verified using the IVIM parameters in the right and left parotid gland (no difference in IVIM parameters were observed between bilateral parotid glands except for C-D values) and the measurements on the largest parotid gland slice and its neighboring upper and lower slices were based on previous research methods; therefore, we believe that automated methods (such as deep learning) for calculating the measurements from all parotid gland slices may be necessary and more accurate.

In summary, this comparative study confirmed that ZOOMit IVIM parameters show higher reproducibility and better performance than those of conventional IVIM parameters in diagnosing early- and mid-stage SS. Especially for patients with mild parotid gland symptoms and normal morphology, the subtle changes in the parotid glands can be detected earlier with ZOOMit IVIM technology. Therefore, ZOOMit IVIM is recommended for use in clinical diagnosis, which contributes to early diagnosis and treatment and bypasses serious disadvantages, including invasiveness and inconsistent LSG biopsy and serological test results [29].

Supplement

The Supplement is available with this article at https://doi.org/10.3348/kjr.2021.0695.

Availability of Data and Material

The datasets generated or analyzed during the study are available from the corresponding author on reasonable request.

Conflicts of Interest

The authors have no potential conflicts of interest to disclose.

Author Contributions

Conceptualization: all authors. Data curation: Yu-Sheng Yu, Hong-Yan Li. Formal analysis: Qing-Qing Zhou, Xue-Song Li. Funding acquisition: Qing-Qing Zhou, Yu-Sheng Yu. Investigation: Qing-Qing Zhou, Wei Zhang, Yu-Sheng Yu, Xue-Song Li. Methodology: Qing-Qing Zhou, Wei Zhang, Yu-Sheng Yu, Xue-Song Li. Project administration: Yu-Sheng Yu, Hong Zhang. Resources: Wei Zhang, Xue-Song Li, Zhen-Zhen He. Software: Qing-Qing Zhou, Xue-Song Li, Liang Wei. Supervision: Yu-Sheng Yu, Hong Zhang. Validation: Qing-Qing Zhou, Hong-Yan Li. Visualization: Qing-Qing Zhou, Wei Zhang. Writing—original draft: Qing-Qing Zhou, Wei Zhang, Hong-Yan Li. Writing—review & editing: Hong Zhang.

ORCID iDs

Qing-Qing Zhou
    https://orcid.org/0000-0002-6699-9617
Wei Zhang
    https://orcid.org/0000-0003-4610-8175
Yu-Sheng Yu
    https://orcid.org/0000-0002-3421-9014
Hong-Yan Li
    https://orcid.org/0000-0002-2429-7158
Liang Wei
    https://orcid.org/0000-0003-2753-2675
Xue-Song Li
    https://orcid.org/0000-0002-2214-0405
Zhen-Zhen He
    https://orcid.org/0000-0001-9425-9555
Hong Zhang
    https://orcid.org/0000-0002-1770-6582

REFERENCES

1. Liu S, Chen W, Wang M, Wu T, Dong L, Pan C, et al.

Quantitative analysis of parotid gland secretion function in Sjögren's syndrome patients with dynamic magnetic resonance sialography. *Korean J Radiol* 2019;20:498-504

2. Chu C, Zhou N, Zhang H, Dou X, Li M, Liu S, et al. Correlation between intravoxel incoherent motion MR parameters and MR nodular grade of parotid glands in patients with Sjögren's syndrome: a pilot study. *Eur J Radiol* 2017;86:241-247

3. Shiboski CH, Shiboski SC, Seror R, Criswell LA, Labetoulle M, Lietman TM, et al. 2016 American College of Rheumatology/ European League Against Rheumatism classification criteria for primary Sjögren's syndrome: a consensus and data-driven methodology involving three international patient cohorts. *Arthritis Rheumatol* 2017;69:35-45

4. Franceschini F, Cavazzana I, Andreoli L, Tincani A. The 2016 classification criteria for primary Sjogren's syndrome: what's new? *BMC Med* 2017;15:69

5. Stefanski AL, Tomiak C, Pleyer U, Dietrich T, Burmester GR, Dörner T. The diagnosis and treatment of Sjögren's syndrome. *Dtsch Arztebl Int* 2017;114:354-361

6. van Stein-Callenfels D, Tan J, Bloemena E, van Vugt RM, Voskuyl AE, Santana NT, et al. The role of a labial salivary gland biopsy in the diagnostic procedure for Sjögren's syndrome; a study of 94 cases. *Med Oral Patol Oral Cir Bucal* 2014;19:e372-e376

7. Chu C, Zhou N, Zhang H, Dou X, Li M, Liu S, et al. Use of T1ρMR imaging in Sjögren's syndrome with normal appearing parotid glands: initial findings. *J Magn Reson Imaging* 2017;45:1005-1012

8. Su GY, Xu XQ, Wang YY, Hu H, Shen J, Hong XN, et al. Feasibility study of using intravoxel incoherent motion MRI to detect parotid gland abnormalities in early-stage Sjögren syndrome patients. *J Magn Reson Imaging* 2016;43:1455-1461

9. Izumi M, Eguchi K, Nakamura H, Nagataki S, Nakamura T. Premature fat deposition in the salivary glands associated with Sjögren syndrome: MR and CT evidence. *AJNR Am J Neuroradiol* 1997;18:951-958

10. Ma G, Xu XQ, Zhu LN, Jiang JS, Su GY, Hu H, et al. Intravoxel incoherent motion magnetic resonance imaging for assessing parotid gland tumors: correlation and comparison with arterial spin labeling imaging. *Korean J Radiol* 2021;22:243-252

11. Zhang L, Murata Y, Ishida R, Ohashi I, Yoshimura R, Shibuya H. Functional evaluation with intravoxel incoherent motion echo-planar MRI in irradiated salivary glands: a correlative study with salivary gland scintigraphy. *J Magn Reson Imaging* 2001;14:223-229

12. Marzi S, Forina C, Marucci L, Giovinazzo G, Giordano C, Piludu F, et al. Early radiation-induced changes evaluated by intravoxel incoherent motion in the major salivary glands. *J Magn Reson Imaging* 2015;41:974-982

13. Zhou N, Chu C, Dou X, Li M, Liu S, Zhu L, et al. Early evaluation of irradiated parotid glands with intravoxel incoherent motion MR imaging: correlation with dynamic contrast-enhanced MR imaging. *BMC Cancer* 2016;16:865

14. Marzi S, Farneti A, Vidiri A, Di Giuliano F, Marucci L, Spasiano F, et al. Radiation-induced parotid changes in oropharyngeal cancer patients: the role of early functional imaging and patient-/treatment-related factors. *Radiat Oncol* 2018;13:189

15. Sim KC, Park BJ, Han NY, Sung DJ, Kim MJ, Han YE. Efficacy of ZOOMit coronal diffusion-weighted imaging and MR texture analysis for differentiating between benign and malignant distal bile duct strictures. *Abdom Radiol (NY)* 2020;45:2418-2429

16. Labounek R, Valošek J, Horák T, Svátková A, Bednařík P, Vojtíšek L, et al. HARDI-ZOOMit protocol improves specificity to microstructural changes in presymptomatic myelopathy. *Sci Rep* 2020;10:17529

17. Attenberger UI, Rathmann N, Sertdemir M, Riffel P, Weidner A, Kannengiesser S, et al. Small field-of-view single-shot EPI-DWI of the prostate: evaluation of spatially-tailored two-dimensional radiofrequency excitation pulses. *Z Med Phys* 2016;26:168-176

18. Liney GP, Holloway L, Al Harthi TM, Sidhom M, Moses D, Juresic E, et al. Quantitative evaluation of diffusion-weighted imaging techniques for the purposes of radiotherapy planning in the prostate. *Br J Radiol* 2015;88:20150034

19. Yıldırım İO, Sağlık S, Çelik H. Conventional and ZOOMit DWI for evaluation of testis in patients with ipsilateral varicocele. *AJR Am J Roentgenol* 2017;208:1045-1050

20. Makula E, Pokorny G, Kiss M, Vörös E, Kovács L, Kovács A, et al. The place of magnetic resonance and ultrasonographic examinations of the parotid gland in the diagnosis and follow-up of primary Sjögren's syndrome. *Rheumatology (Oxford)* 2000;39:97-104

21. Le Bihan D, Breton E, Lallemand D, Aubin ML, Vignaud J, Laval-Jeantet M. Separation of diffusion and perfusion in intravoxel incoherent motion MR imaging. *Radiology* 1988;168:497-505

22. Gatidis S, Graf H, Weiß J, Stemmer A, Kiefer B, Nikolaou K, et al. Diffusion-weighted echo planar MR imaging of the neck at 3 T using integrated shimming: comparison of MR sequence techniques for reducing artifacts caused by magnetic-field inhomogeneities. *MAGMA* 2017;30:57-63

23. Schneider R, Ritter D, Haueisen J, Pfeuffer J. Novel 2DRF optimization framework for spatially selective Rf pulses incorporating B1, B0 and variable-density trajectory design. Proceedings of the 20th Scientific Meeting, International Society for Magnetic Resonance and Medicine; 2012 May 5-11; Melbourne, Australia; 2012; p.3454

24. Schneider R, Ritter D, Haueisen J, Pfeuffer J. Evaluation of 2DRF echo-planar pulse designs for parallel transmission. Proceedings of the 20th Scientific Meeting, International Society for Magnetic Resonance and Medicine; 2012 May 5-11; Melbourne, Australia; 2012; p.3459

25. Jia QJ, Zhang SX, Chen WB, Liang L, Zhou ZG, Qiu QH, et al. Initial experience of correlating parameters of intravoxel incoherent motion and dynamic contrast-enhanced magnetic resonance imaging at 3.0 T in nasopharyngeal carcinoma. *Eur*

Radiol 2014;24:3076-3087
26. Bologna SB, Cavalcante WS, Florezi GP, Souza MM, Nico MMS, Lourenço SV. Distinct salivary gland features in Sjögren's syndrome and lupus erythematosus sialadenite. *Am J Dermatopathol* 2020;42:407-413
27. Wicheta S, Van der Groen T, Faquin WC, August M. Discrepancies in interpretation of the minor salivary gland biopsy in the diagnosis of Sjögren syndrome. *J Oral Maxillofac Surg* 2019;77:1628-1635

28. Zhang SX, Jia QJ, Zhang ZP, Liang CH, Chen WB, Qiu QH, et al. Intravoxel incoherent motion MRI: emerging applications for nasopharyngeal carcinoma at the primary site. *Eur Radiol* 2014;24:1998-2004
29. Bredahl SK, Reibel J, Pedersen AML. Value of multilevel sectioning of labial salivary gland biopsies in the diagnosis of Sjögren's syndrome. *Oral Surg Oral Med Oral Pathol Oral Radiol* 2021;131:85-91